# Correlations of stripe phase in one-dimensional spin-orbit coupled Bose gas

Clemens Staudinger,[1,*] Martin Panholzer,[1,2] and Robert E. Zillich[1,†]
[1]*Institute for Theoretical Physics, Johannes Kepler University, Altenbergerstrasse 69, 4040 Linz, Austria*
[2]*Uni Software Plus GmbH, Linzer Strasse 6, 4320 Perg, Austria*

(Received 26 February 2021; accepted 1 June 2021; published 25 June 2021)

We investigate the effects of interaction for the stripe phase of a homogeneous one-dimensional Bose gas with laser-induced Raman spin-orbit coupling (SOC) and Zeeman splitting, for a wide range of densities. In order to account for quantum fluctuations, important in one dimension for low densities close to the Tonks-Girardeau limit, we use a variational method based on the hypernetted-chain Euler-Lagrange optimization of a Jastrow-Feenberg ansatz for the many-body wave function. For strong coupling we observe significant deviations from mean-field results not only quantitatively but also qualitatively. The main interest of this paper lies in the interplay and competition between interaction-induced pair correlations and the SOC-induced density oscillations of the stripe phase. We explain the increase in wave number of this density oscillation with increasing interaction due to an effective attraction between particles in the many-body system.

DOI: 10.1103/PhysRevResearch.3.023245

## I. INTRODUCTION

Spin-orbit coupling (SOC) can connect the spin of a particle not just with its orbital angular momentum, but also its linear momentum. This latter case has been demonstrated by Rashba and Dresselhaus during the course of the last century [1,2]. However, experimental studies of such systems have been limited to the narrow range of coupling strengths in solids. In ultracold quantum gases the type of SOC as well as its strength can be engineered by external fields in the laboratory. The illumination of an ultracold Bose gas with Raman lasers couples the hyperfine states of the atoms of the gas. This results, for example, in a system with equal Rashba- and Dresselhaus-SOC and thus breaks rotational symmetry [3–6]. In addition a Zeeman term is added, which mixes the spin components. Although, such a one-dimensional SOC will be the primary concern of this work, we want to point out that numerous other schemes of SOC have been theoretically proposed or experimentally realized like pure Rashba coupling [7,8] in 2D with a Dirac point or isotropic SOC in three dimensions [9]. Most SOC systems possess a degenerate ground state, which gives rise to a rich phase diagram already in the noninteracting case. The effect of interactions has been extensively studied within mean-field [10–15] as well as quantum Monte Carlo (QMC) approaches [16–20]. Additionally, the Hubbard model for lattice systems has been modified to include SOC [21]. In particular for Raman SOC with Zeeman splitting the single-particle dispersion depending on the strength of the Zeeman splitting possesses either one minimum at the center of the dispersion or two minima, which are displaced symmetrically. Therefore, particles can populate each of the available minima (single-minimum and polarized phase) or be in a superposition of two minima (stripe phase), which gives rise to a density modulation [22–26]. We stress that this lattice-like density oscillation is a self-organized stripe phase, not imposed by an optical lattice. In addition it was proven experimentally that the stripe phase possesses supersolid properties [26,27]. The phase transitions of a SOC system were even investigated at finite temperature [23,28] and dynamically [29]. Alternative schemes using external potentials have been proposed, which facilitate the detection of the stripes in the experiment [22,27,30]. In this work we focus on the stripe phase in a spin-unpolarized system (i.e., equal population of internal pseudospin states labeled $|\uparrow\rangle$ and $|\downarrow\rangle$). In spite of mean-field approaches providing valuable insight in the behavior of a Bose gas with SOC, those approaches significantly lack the ability to describe strongly correlated systems. This shortcoming becomes especially apparent in one-dimensional systems, where correlations are known to play an even more significant role than in higher dimensions and are stronger for lower densities [31]. In this paper we use the hypernetted-chain Euler-Lagrange (HNC-EL) method [32,33], which has been shown to account for correlations also in 1D [34,35]. We use an approximation of the inhomogeneous HNC-EL method [36,37], derived for periodic systems in Ref. [38].

## II. METHODOLOGY

For a boson with mass $m$ we start with the single-particle Hamiltonian, which apart from the kinetic term contains a Raman SOC term that couples the linear momentum and the spin by the constant $\alpha$ and a Zeeman term, which acts

*clemens.staudinger@jku.at
†robert.zillich@jku.at

only on the spin with the strength $\Omega$ given by the Raman coupling strength. Following the notation of Ref. [12], the single-particle Hamiltonian is

$$\hat{H}_1 = \frac{\hat{p}_x^2}{2m} + \alpha \hat{p}_x \hat{\sigma}_z + \Omega \hat{\sigma}_x \,. \tag{1}$$

For the calculations we use the units $k_L = 2\pi/\lambda$, $E_L = \hbar^2 k_L^2/2m$, $\alpha = 2E_L/\hbar k_L$, where $\lambda$ is the wave length of the Raman laser used in the experimental realization of SOC. In our calculations we operate at interparticle distances $r_s = 5, 10/k_L$ somewhat larger than 3D experiments [27] ($\lambda = 1064\,\mathrm{nm} \rightarrow k_L = 0.0059\,\mathrm{nm}^{-1}$ and $r_s = 1/\rho_{3D}^{1/3} = 1.11/k_L$) and similar to QMC simulations [20] ($r_s = 6.46/k_L$). The many-particle Hamiltonian of an $N$-particle system with SOC and interaction $v$ is given by

$$\hat{H} = \sum_{i=1}^{N} \hat{H}_i + \sum_{i<j} v(|x_i - x_j|) \,, \tag{2}$$

with $\hat{H}_i$ from Eq. (1). In this work we assume a spin-independent interaction modelled by $v(x) = V_0 \exp[-(x/(bk_L))^2]$, from which the scattering length $a_s$ can be calculated [39]. For comparing with mean-field results the coupling strength in 1D $g_c = -4E_L/(a_s k_L^2)$ [40]. We make a variational Jastrow-Feenberg ansatz for the ground state, containing two-body correlations $u(x_i, x_j)$, which account for quantum fluctuations, and one-body functions $\psi(x_i, s_i)$ [36,38,41,42]

$$\Psi(x_1, s_1, \ldots, x_N, s_N) = \prod_{i<j} \exp\left[\frac{u(x_i, x_j)}{2}\right] \prod_{i=1}^{N} \psi(x_i, s_i). \tag{3}$$

Here $s \in [0, 2\pi]$ is the continuous spin coordinate [43]. Only $\psi$ depends on the spin, while we consider no explicit spin-dependence for the correlations $u(x_i, x_j)$; they only indirectly depend on the spin via the minimization of the energy, which contains the SOC terms, see below. A generalization to spin-dependent interactions would require spin-dependent correlations, which we currently work on. On the other hand, if we omitted $u(x_i, x_j)$ completely, we would revert to the mean-field approximation.

According to Ritz' variational principle we obtain the optimal ground state by solving the Euler-Lagrange equations $\delta e/\delta g(x, x') = 0$ where the energy per particle $e = \frac{1}{N}\frac{\langle\Psi|\hat{H}|\Psi\rangle}{\langle\Psi|\Psi\rangle}$ is given by

$$e = \frac{\hbar^2}{8mN} \int dx\, \rho(x) |\nabla \ln \rho(x)|^2 + \frac{1}{2N} \int dx \int dx'\, \rho(x)\rho(x') g(x, x') v_{JF}(x, x') + \varepsilon_0, \tag{4}$$

with the Jackson-Feenberg interaction

$$v_{JF}(x, x') = v(|x - x'|) - \frac{\hbar^2}{8m}\left[\frac{1}{\rho(x)} \nabla \rho(x) \nabla + \frac{1}{\rho(x')} \nabla' \rho(x') \nabla'\right] u(x, x'), \tag{5}$$

the energy of the noninteracting system $\varepsilon_0$ and the spin-averaged single-particle density $\rho(x)$. $g(x, x')$ is the pair-distribution function defined as

$$g(x_1, x_2) = \frac{(2\pi)^{-N} N(N-1)}{\langle\Psi|\Psi\rangle \rho(x_1)\rho(x_2)} \int dx_3 ds_1 \ldots dx_N ds_N |\Psi|^2. \tag{6}$$

Closure is provided by the HNC/0 relation between $g(x, x')$ and $u(x, x')$ [44], where we omit the so-called elementary diagrams. The single-particle functions $\psi(x, s)$ [and thus the density $\rho(x)$] can also be obtained by optimization of the energy. However, here we choose an approximate approach [38]. Based on the stripe phase density of the noninteracting system (see Appendix), we account for interactions introducing two variational parameters $(q, A)$, which scale the wave number and amplitude of the stripe oscillation and are used to minimize the energy. Hence we make the ansatz for the density

$$\rho(x; q, A) = \rho_0[1 + A\cos(2qx)] \,, \tag{7}$$

with mean density $\rho_0$. Note that the density in the absence of interaction also possesses this functional form. With this ansatz for the density the energy of the noninteracting system becomes

$$\frac{\varepsilon_0(q, A)}{E_L} = \left(\frac{q}{k_L}\right)^2 - A\frac{\Omega}{E_L} - 2\frac{q}{k_L}\sqrt{1 - A^2} \,. \tag{8}$$

## III. ENERGY, DENSITY OSCILLATION, SPIN POLARIZATION

In panel (a) of Fig. 1 we compare the energy obtained with the HNC-EL/0 method with the mean-field expression $e_{MF}/E_L = -\Omega^2/(4FE_L^2) - 1 + (g_c\rho_0)/(4E_L)$, with $F = 1 + (g_c\rho_0)/(4E_L)$ [12]. Being an improved variational ansatz compared to mean-field, HNC-EL/0 gives a lower energy, in accordance with Ritz' principle. The shift in energy is very small for weak interactions, but becomes huge for strong interactions (up to 50% for $\rho_0 = 0.2k_L$ and $g_c = 9.28E_L/k_L$), where the inclusion of correlations proves to be crucial. For $\rho_0 = 0.2k_L$ and $g_c = 9.28E_L/k_L$ the system is already close to the Tonks-Girardeau limit ($g_c \rightarrow \infty$) of impenetrable bosons [45], and $e - E_{min}$ [inset in panel (a) of Fig. 1] is reaching values on the order of the Tonks-Girardeau energy $e_{TG} \approx 0.13E_L$ (no SOC included) [46,47]. Here $E_{min}/E_L = -1 - \Omega^2/(4E_L^2)$ is the minimum of the eigenenergy of Eq. (1). The exact energy for Tonks-Girardeau with SOC is not known, but could be obtained with Monte Carlo simulations.

A comparison of mean-field energies [12] of the stripe phase, single-minimum phase, and separated phase for a Bose gas with spin-independent interaction predicts that it is energetically favorable that the spins separate into polarized domains for $\Omega/E_L < 2$; the stripe phase is not favored for any value of $\Omega$. Our HNC-EL calculations, which account for quantum fluctuations in the variational ansatz, indicate that the stripe phase is metastable nonetheless, at least in 1D, see illustration in Fig. 4 in the Appendix. It is energetically favored compared to the single-minimum phase except for large $\Omega$, as also described in the Appendix (Fig. 6). The energy comparison with the separated phase would require spin-sensitive correlations $u$ in the ansatz (3), which we plan to account for in future work. Such an extension of our approach will allow to draw a full phase diagram of the ground state.

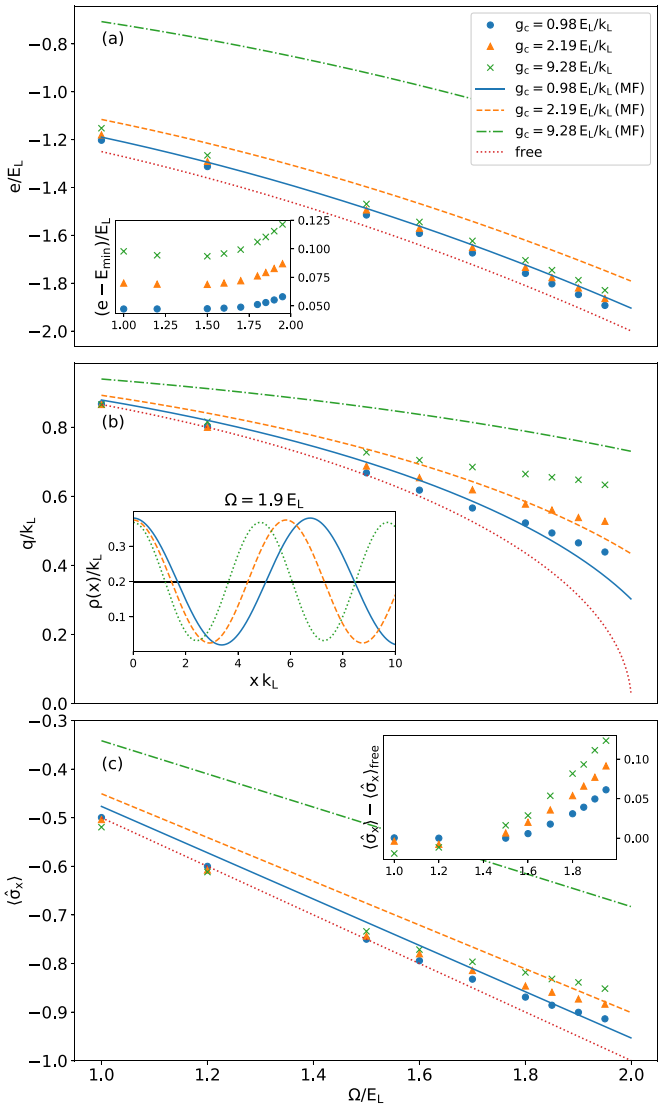


FIG. 1. Energy per particle $e/E_L$ (a), wave number $q/k_L$ (b), and transverse spin polarization $\langle\hat{\sigma}_x\rangle$ (c) as a function of $\Omega$ for different $g_c$ and $\rho_0 = 0.2k_L$. The symbols are the HNC-EL/0 results, Eqs. (8), (7), and (9) and the lines depict the corresponding mean-field results. (a) For low $g_c$ there is only a slight difference between the energies of the two methods, whereas for larger $g_c$ the deviation increases. The inset shows the difference of the HNC-EL/0 energy to the energy of the free system. (b) Especially, for high $\Omega$ the mean-field approximation deviates strongly from the HNC-EL/0 result for $q/k_L$. The inset shows an example of the density $\rho(x)$; the wave number grows and the amplitude falls with growing $g_c$. (c) The inset shows the difference of the HNC-EL/0 result for $\langle\hat{\sigma}_x\rangle$ to the free results. Especially for high $\Omega$, HNC-EL/0 predicts a smaller $\langle\hat{\sigma}_x\rangle$, which means that the polarization is suppressed.

Interactions affect the single-particle dispersion and therefore alter the wave number $q/k_L$ of the density oscillation, as shown in panel (b) of Fig. 1. For low values of $\Omega$ the wave number follows the result for the noninteracting system (dotted line), because the influence of SOC is small, as we will see in the discussion of the pair-distribution function at low $\Omega$. For large $\Omega$ one notices a significant shift of the wave number to higher values compared to the noninteracting solution. This means that although without interaction the density oscillation would vanish in the limit $\Omega \to 2E_L$, the interaction preserves the oscillation. The value of $\Omega$ at which this increase in wave number starts to occur is lower for high interaction strength. The mean-field result $q_{MF}/k_L = \sqrt{1 - (\Omega/(2FE_L))}$ [12] also predicts an increased wave number due to interaction, however, for strong interaction the wave number is overestimated. Also, $q_{MF}/k_L$ tends to be steeper as function of $\Omega$ than the HNC-EL/0 result. The origin of the increase of $q/k_L$ with interaction strength will become clear in the discussion of the pair-distribution function $g(x, x')$ below. The density $\rho(x)$ [inset in panel (b) of Fig. 1] shows that with increasing $g_c$ the amplitude of the density oscillation decays.

The transverse spin polarization per particle $\langle\hat{\sigma}_x\rangle$ is $-1$ for the single-minimum phase but has a smaller magnitude in the stripe phase. In the mean-field approach it is given as $\langle\hat{\sigma}_x\rangle_{MF} = -\Omega/(E_L F)$ [12]. In HNC-EL/0 we evaluate the expression (see the Appendix for a derivation)

$$\langle\hat{\sigma}_x\rangle = -A\,. \tag{9}$$

While $\langle\hat{\sigma}_x\rangle_{MF}$ has a purely linear dependence on $\Omega$, this is not true for large $\Omega$ according to the HNC-EL/0 results, as can be seen in panel (c) of Fig. 1 and its inset. In this regime quantum fluctuations add non-linear contributions to the polarization, which prove once more that a mean-field approach is no longer applicable.

The local orientation of the spin, the spin structure, has been investigated in previous studies of up to four, impenetrable ($g_c \to \infty$) bosons or fermions in a 1D trap [48,49]. The spin structure is calculated via the expectation values of the operators $\hat{\sigma}_\zeta(x) = \sum_i^N \hat{\sigma}_{\zeta,i}\delta(x - x_i)$ with $\zeta = x, y, z$. With our ansatz (3) $\langle\hat{\sigma}_z(x)\rangle$ vanishes and the spin structure must follow the density structure, with

$$\langle\hat{\sigma}_x(x)\rangle = -\rho_0[A + \cos(2qx)], \tag{10}$$

$$\langle\hat{\sigma}_y(x)\rangle = -\rho_0\sqrt{1 - A^2}\sin(2qx)\,. \tag{11}$$

These HNC-EL/0 results for a large $g_c = 9.28E_L/k_L$ are depicted alongside mean-field results deduced from Ref. [12] in Fig. 2. Our results deviate from mean-field predictions, which is even more significant for a high value of $\Omega = 1.9E_L$ [panel (b) in Fig. 2]. The component $\langle\hat{\sigma}_x(x)\rangle$ is in phase with the density while $\langle\hat{\sigma}_y(x)\rangle$ is shifted by $\pi/2$. This is qualitatively the same result found for two bosons in Ref. [49] (see Fig. 4 therein). This phase shift results in an oscillating movement of the spin vector (arrows in Fig. 2). For $\Omega = 1.9E_L$ the Zeeman effect dominates and the spin points mostly in the negative $x$ direction.

## IV. PAIR-DISTRIBUTION FUNCTION

We have seen from the comparisons between our HNC-EL/0 results and the mean-field results that quantum fluctuations have a significant influence on energy, density modulation and polarization of a 1D Bose gas with SOC. In order to *understand* the physical origin of these effects, we investigate the pair-distribution function $g(x, x')$ (6). An ultracold Bose gas in the stripe phase is characterized by two length scales, which are the average inter-particle distance $1/\rho_0$ and the period of the density oscillation $\pi/q$. The ratio

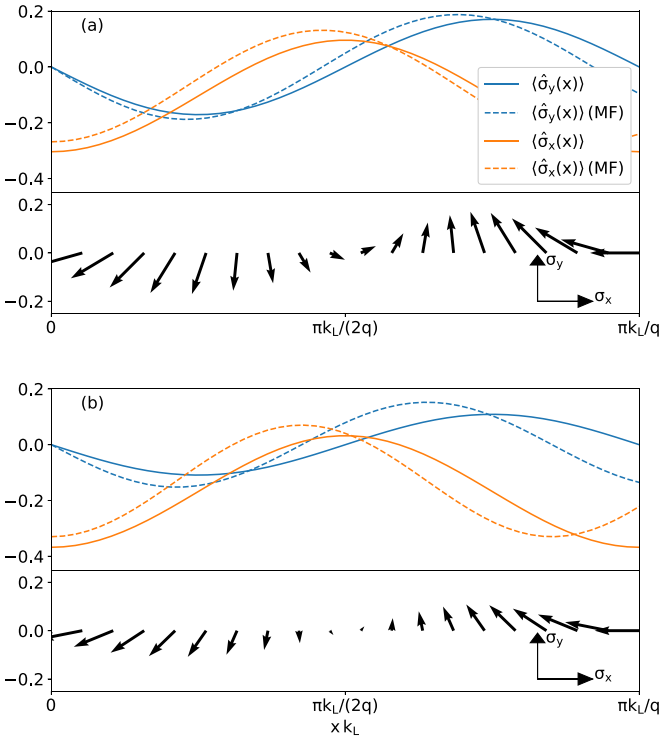


FIG. 2. Components of the spin structure $\langle\hat{\sigma}_y(x)\rangle$ (blue) and $\langle\hat{\sigma}_x(x)\rangle$ (orange) and orientation of the spin vector $(\langle\hat{\sigma}_x(x)\rangle, \langle\hat{\sigma}_y(x)\rangle)$ (arrows below) within the first period of the density oscillation for $\rho_0 = 0.2k_L$, $g_c = 9.28E_L/k_L$ as well as $\Omega = 1E_L$ (a) and $\Omega = 1.9E_L$ (b). The dashed lines are the corresponding mean-field results.

between the two values is an indicator for the interplay of interaction and SOC. In Figs. 3 (a) and 3(b) we show $g(x, x')$ for two cases at a mean density of $\rho_0 = 0.2k_L$: a 1D Bose gas where the interaction dominates (a) and a 1D Bose gas where SOC dominates (b).

In the first case, $\Omega = 0.5E_L$ is small and $g_c = 9.28E_L/k_L$ is large, therefore $g(x, x')$ is close to $g_{\Omega=0}(x, x')$ [dotted dashed line in Fig. 3(a)], apart from small oscillations (note that for $\Omega = 0$, the system is homogeneous). The formation of these oscillations can be understood as periodically changing correlations (i.e., more or less repulsion) between two particles for certain distances.

The second case, where SOC dominates, is realized when the interparticle distance and the period of the oscillation are on the same scale (i.e., $1/\rho_0 \sim \pi/q$ and the effects of SOC and interaction overlap and enhance each other) or if the period is larger. Now all maxima are occupied with approximately one particle. This regime is reached for either large Zeeman splittings, weak interactions, or high densities. The case of large $\Omega = 1.9E_L$ is shown in Fig. 3(b). Here $g(x, x')$ possesses strong oscillations with the same period as the density oscillation—for the small $\Omega$ value of panel (a), this effect was only visible as the small oscillations in $g(x, x')$ about the $\Omega = 0$ result. Now SOC has a strong influence on the correlations, and $g(x, x')$ deviates significantly from the homogeneous $\Omega = 0$ result. Also, since each density maximum is approximately occupied by one particle, the enhancement of $g(x, x')$ is maximal if the distance between two particles is a multiple of the period.

Even more interesting is the situation at a lower mean density $\rho_0 = 0.1k_L$, but also lower coupling strength $g_c = 0.98E_L/k_L$. Here $\rho(x)$ is almost zero in its minima and the oscillations in $g(x, x')$ become step-like, starting at $x' = \pi/(2q)$ for all $x$ [panel (c) of Fig. 3]. $g(x, x')$ varies little near density maxima, but sharply increases at density minima. This behavior might seem strange at first, but one has to keep in mind that SOC causes oscillations, which turn a weakly correlated system into a strongly correlated one, similarly to optical lattices: Particles want to occupy different density maxima, in order to minimize their interaction. This is reflected by $g(x, x')$ being very small if two particles would be found in the same maximum. However, if they are located in different maxima, the exact position there matters little, because interactions are weak between neighboring density maxima. We observe here the gradual transition to a lattice Hamiltonian. Note that, despite the weakness of the interaction in Fig. 3(c), a mean-field description is not valid, at least for low density.

With increasing interaction the step-like behavior of $g(x, x')$ becomes less pronounced, because the interaction suppresses the effects of SOC, see Fig. 3(b). In the Appendix in Fig. 9 we show $g(x, x')$ for $\Omega = 1.9E_L$, $\rho_0 = 0.2k_L$ as in Fig. 3(b) but for a lower coupling strength of $g_c = 0.98E_L/k_L$, which represents an intermediate situation between the results of the panels (b) and (c) of Fig. 3.

With the optimized pair-distribution function we are able to understand the wave number shift from Fig. 1(c). Recall that for large Zeeman splitting $\Omega$, one observes an increase of the wave number of the density oscillation with increasing interaction strength. In order to understand the reason for this increase we show the effective interaction between two particles, $V_{\text{eff}}(x, x') = v(|x - x'|) + w_I(x, x')$ in Fig. 3(d) for the parameters used in Fig. 3(b), where $w_I(x, x')$ is the induced interaction mediated by exchange of elementary excitations [50]. Unlike the bare interaction $v(|x - x'|)$, the effective interaction is partially attractive and possesses a distinct minimum for a distance between $x$ and $x'$, which is much smaller than the distance between maxima of the density oscillation and is deepest for high $g_c$. The wave number that is actually observed with interaction is a compromise between the attraction from the effective interaction and the wave number of the SOC-induced stripe phase without interaction. Note that qualitatively this effect is already present in mean-field calculations, which however do not give an explanation.

## V. CONCLUSIONS

In summary, quantum fluctuations, accounted for by pair correlations in the many-body wave function, lead to significant corrections with respect to mean-field results for all properties of a spin-orbit coupled 1D Bose gas. The stronger the interaction between the particles, the more our HNC-EL/0 results for energy, density oscillation wave number, and polarization differ from the corresponding mean-field results, because for strong interactions or low density a 1D Bose gas enters the Tonks-Girardeau regime. In particular the lower value of the energy per particle is comparable to the energy of a non-SOC Bose gas in the Tonks-Girardeu limit of infinite

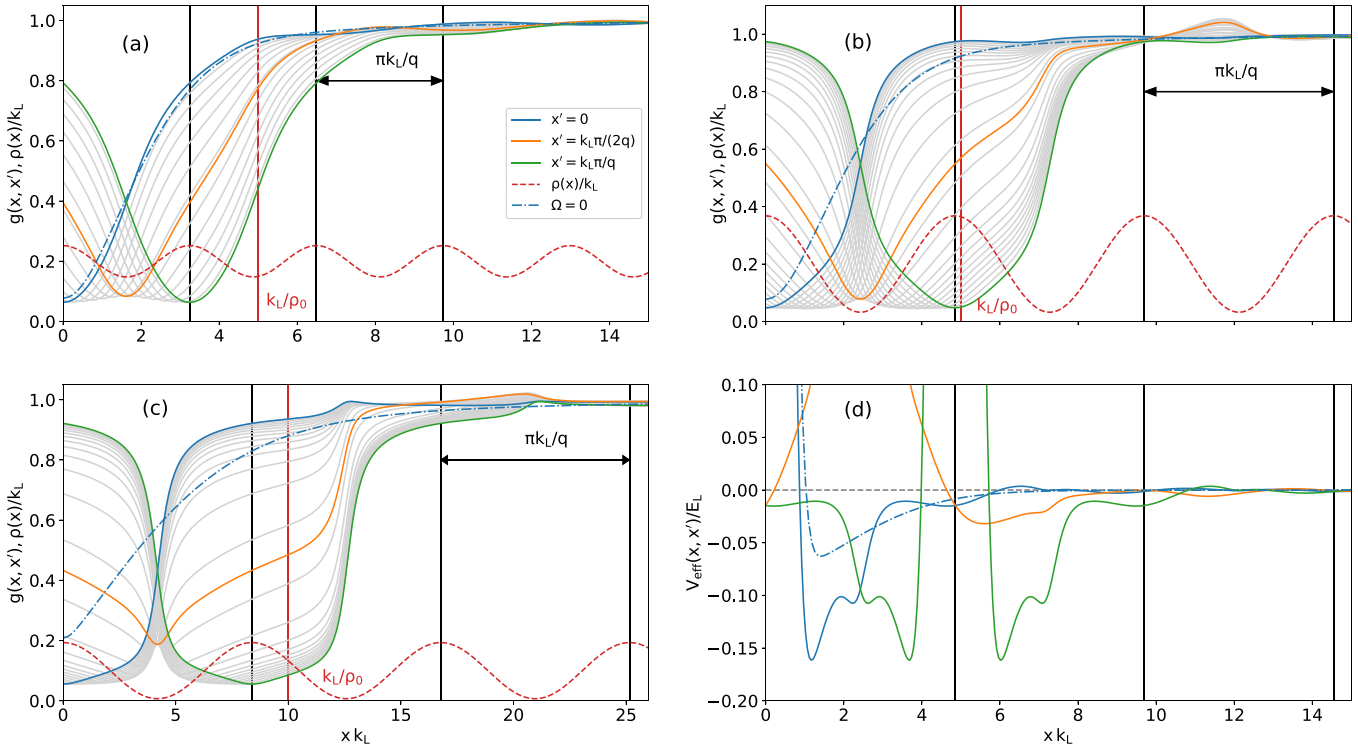


FIG. 3. Pair-distribution function $g(x, x')$ [(a),(b),(c)] and $V_{\rm eff}(x, x')$ (d) as a function of $x$ for different $x'$ for Zeeman splitting $\Omega = 0.5E_{\rm L}$, density $\rho_0 = 0.2k_{\rm L}$ and coupling strength $g_{\rm c} = 9.28E_{\rm L}/k_{\rm L}$ (a), $\Omega = 1.9E_{\rm L}$, $\rho_0 = 0.2k_{\rm L}$ and $g_{\rm c} = 9.28E_{\rm L}/k_{\rm L}$ (b), and $\Omega = 1.9E_{\rm L}$, $\rho_0 = 0.1k_{\rm L}$ and $g_{\rm c} = 0.98E_{\rm L}/k_{\rm L}$ (c). The solid blue line is for $x' = 0$ (beginning of the unit cell), the orange line is $x' = \pi/(2q)$ (center of the unit cell), and the green line is $x' = \pi/q$ (end of the unit cell), the grey lines are values of $x'$ in between. The single-particle density is the dashed red line with its periodicity marked by the black vertical lines. The red vertical line marks the mean distance between the particles. (a) For small $\Omega$ and large $g_{\rm c}$, $g(x, x')$ deviates only slightly from the $\Omega = 0$ result (blue dotted dashed line) because the interaction dominates. (b) For high $\Omega$, a significant deviation from the result without Zeeman splitting is visible, the influence of SOC on the correlations is growing. (c) For large $\Omega$ and small $g_{\rm c}$, the correlations are dominated by SOC and $g(x, x')$ looks very different from the case of $\Omega = 0$. The particles are strongly localized in their unit cells, which leads to a steep increase of $g(x, x')$ when two particles are found in different unit cells. (d) The effective interaction possesses a pronounced minimum within the first unit cell.

repulsion. We predict that the stripe phase is metastable in a 1D Bose gas even for spin-independent interactions and we hope that our findings spark interest in experimental preparation and the investigation of the stability of such systems. In this context it should be mentioned that in combination with a trap they can indeed support a striped ground state [51–53]. Via the pair-distribution $g(x, x')$ we are able to explain the interaction-induced wave number shift of the density oscillation with respect to the noninteracting wave number, which we can attribute to the induced attraction between bosons mediated by elementary excitations. Our results for $g(x, x')$ show that a SOC Bose gas in 1D is a rich and interesting model system because of the concurrence of and competition between two quantum fluctuations effects: The lattice imposed by SOC can turn the Bose gas into a strongly correlated system even for weak interaction; strong interaction or low density drives the Bose gas to the Tonks-Girardeau limit, again rendering the system strongly correlated.

For future work we will perform full optimization of the single-particle density [36,54] as well as the approximate inclusion of triplet correlations in the trial wave function (3) and elementary diagrams in the HNC relation [55], and investigate excitations beyond the mean-field level [3,6,56–58] using the correlated basis function method [32,59–61]. Finally, an extension to spin-dependent correlations in the ansatz (3) would allow for an investigation of the complete phase diagram for spin-dependent interactions.

## ACKNOWLEDGMENTS

We acknowledge support from the Austrian Agency for International Cooperation in Education and Research, OeAD (Project No. HR 07/2018) and fruitful discussions with Eckhard Krotscheck, Jiawei Wang, Ferran Mazzanti, Andrii Gudyma, and Leandra Vranješ Markić. Supported by Johannes Kepler Open Access Publishing Fund.

## APPENDIX

### 1. Ansatz for the single-particle density

We perform a spin rotation on the Hamiltonian (1) and obtain

$$\hat{\tilde{H}}_1 = \frac{\hat{p}_x^2}{2m} + \alpha \hat{p}_x \hat{\sigma}_{\rm y} + \Omega \hat{\sigma}_{\rm z}\,. \tag{A1}$$

Its eigenenergies and eigenfunctions are

$$E_\pm = \frac{\hbar^2 k^2}{2m} \pm \sqrt{\alpha^2\hbar^2k^2 + \Omega^2} \tag{A2}$$

$$\tilde{\psi}_\pm(x,s) = \frac{\exp(\imath kx)}{\sqrt{L}} \times \left[\left(\imath \underbrace{\frac{(-\Omega \mp \sqrt{\alpha^2\hbar^2k^2+\Omega^2})}{\alpha\hbar k}}_{:=\beta_\pm(k)}\right) e^{\imath s} + e^{-\imath s}\right], \tag{A3}$$

with normalization length $L$. The minimum of the dispersion relation is obtained as

$$\frac{q_{\min}}{k_L} = \pm\frac{1}{2}\sqrt{4 - \left(\frac{\Omega}{E_L}\right)^2}, \qquad \frac{E_{\min}}{E_L} = -1 - \frac{\Omega^2}{4E_L^2}. \tag{A4}$$

The single-particle wave function in a superposition of the two states in the minima of the dispersion relation is

$$\tilde{\psi}(x,s) = \sqrt{\frac{2}{L(\beta^2+1)}} \times \left[-\beta \sin(|q_{\min}|x)e^{\imath s} + \cos(|q_{\min}|x)e^{-\imath s}\right], \tag{A5}$$

with $\beta := \beta_-(q_{\min}) = (2 - \Omega/E_L)/\sqrt{4 - (\Omega/E_L)^2}$ and where $x$ is the spatial coordinate and $s$ is the spin coordinate [43]. We construct the single-particle density as

$$\rho(x) = \frac{1}{2\pi}\int_0^{2\pi} ds\, |\psi(x,s)|^2 = \frac{1}{2\pi}\int_0^{2\pi} ds\, |\tilde{\psi}(x,s)|^2. \tag{A6}$$

The evaluation of this expression leads to

$$\rho(x) = \frac{2\rho_0}{\beta^2+1}\left[1 + \sin^2\left(|q_{\min}|x\right)\left(\beta^2 - 1\right)\right], \tag{A7}$$

with mean density $\rho_0$. To account for the interaction of the particles in the system we allow a displacement of the wave number in the minimum of the dispersion and replace $q_{\min} \to q := \omega q_{\min}$. This replacement also leads to an altered $\beta$. Here we allow for further freedom of the ansatz and write

$$\beta(\gamma) = \sqrt{1 - \frac{2\Omega/E_L}{\Omega/E_L + \sqrt{(\Omega/E_L)^2 - \gamma^2\left((\Omega/E_L)^2 - 4\right)}}}, \tag{A8}$$

where we introduced a second variational parameter $\gamma$ instead of $\omega$. Note that we could have chosen amplitude $A$ and wave number $q$ of the oscillation as variational parameters from the very beginning. However, the line of argumentation presented here gives a justification for the functional form of the ansatz, which is motivated by the noninteracting single-particle result and not just a guess. In addition, $\omega$ and $\gamma$ are of the same order of magnitude.

### 2. Calculation of the energy

We calculate the energy using coupling constant integration, which requires the energy of the noninteracting system $\varepsilon_0(\omega, A)$ and the potential energy $U$ as a function of a coupling constant $c$ [here the interaction is scaled: $v(x) \to cv(x)$]. In order to calculate the potential energy per particle for a periodic system we start with the well known expression for the potential energy

$$U = \frac{1}{2}\int_{-\infty}^{\infty} dx \int_{-\infty}^{\infty} dx' v(|x-x'|)\rho_2(x,x'), \tag{A9}$$

where $\rho_2(x,x')$ is the pair-density, which can be expressed in terms of the density and the pair-distribution function $\rho_2(x,x') = \rho(x)\rho(x')g(x,x')$. In the stripe phase these functions are periodic:

$$g(x+na, x'+ma) = g(x,x') \tag{A10}$$

$$\rho(x+na) = \rho(x), \tag{A11}$$

where $n, m \in \mathbb{Z}$ and $a$ is the length of a unit cell. Making use of this periodicity one arrives at the expression

$$\frac{U}{N} = \frac{1}{2\rho_0 a}\int_{-\infty}^{\infty} dx \int_0^a dx' v(|x-x'|)\rho(x)\rho(x')g(x,x'), \tag{A12}$$

where $a$ is the length of a unit cell. In order to obtain the total energy one performs an integration over $c$:

$$e = \int_0^1 dc\, \frac{U(c)}{N}. \tag{A13}$$

Note that this method requires multiple evaluations of $g(x,x')$ and the corresponding potential energy. Alternatively, one can directly calculate the energy functional [Eq. (4) in the main text].

Figure 4 shows the energy as a function of the parameters $q$ and $A$ in the density [see Eq. (4) in the main text] along with the numerically calculated minimum (red dot). It is important to note that no additional minima are present in this calculation, which was checked by calculating the energy on a grid for a wide range of parameters $A$ and $q$.

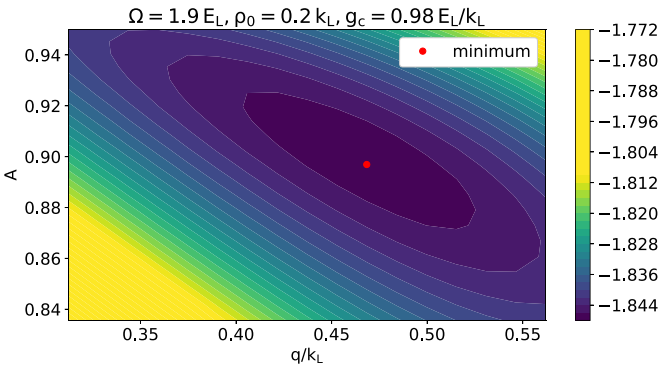


FIG. 4. Energy per particle as a function of $q$ and $A$ for $\Omega = 1.9E_L$, $\rho_0 = 0.2k_L$ and $g_c = 0.98E_L/k_L$. The red dot represents the minimum of the energy surface and thus marks the final result of the energy calculation.

### 3. Calculation of $\langle\hat{\sigma}_x\rangle$

The transverse spin polarization is calculated as the expectation value of $\hat{\sigma}_x$, which is given as

$$\langle\hat{\sigma}_x\rangle = \frac{1}{N}\frac{\langle\Psi|\sum_i \hat{\sigma}_{x,i}|\Psi\rangle}{\langle\Psi|\Psi\rangle}, \tag{A14}$$

where $\Psi$ is the variational wave function (3) in the main text. The general definition of the spin-averaged single-particle density is

$$\rho(x_1) = \frac{N}{(2\pi)^N\langle\Psi|\Psi\rangle}\int_0^{2\pi} ds_1\ldots ds_N \times \int dx_2\ldots dx_N|\Psi(x_1,\ldots,x_N,s_1,\ldots,s_N)|^2, \tag{A15}$$

Let us first observe the expectation value of $\hat{\sigma}_{z,i}$ with respect to the rotated single-particle wave function Eq. (A5) and the spin. We can explicitly calculate that

$$\frac{1}{2\pi}\int_0^{2\pi} ds_i\tilde{\psi}^*(x_i,s_i)\hat{\sigma}_{z,i}\tilde{\psi}(x_i,s_i) = \frac{\beta^2\sin^2(qx_i)-\cos^2(qx_i)}{\beta^2\sin^2(qx_i)+\cos^2(qx_i)}\frac{1}{2\pi}\int_0^{2\pi} ds_i|\psi(x_i,s_i)|^2 \tag{A16}$$

This result will prove to be very useful, because also in the many particle expectation value $\hat{\sigma}_x$ acts only on the single-particle functions. With this result we can write

$$\langle\hat{\sigma}_x\rangle = \frac{1}{\langle\Psi|\Psi\rangle}\int_{-\infty}^{\infty} dx_1\frac{\beta^2\sin^2(qx_1)-\cos^2(qx_1)}{\beta^2\sin^2(qx_1)+\cos^2(qx_1}\times\frac{1}{(2\pi)^N}\int_0^{2\pi} ds_1\ldots ds_N\int dx_2\ldots dx_N|\Psi|^2. \tag{A17}$$

Using the definition of the single-particle density from Eq. (A15) we can further simplify

$$\langle\hat{\sigma}_x\rangle = \frac{1}{N}\int_{-\infty}^{\infty} dx\frac{\beta^2\sin^2(qx)-\cos^2(qx)}{\beta^2\sin^2(qx)+\cos^2(qx)}\rho(x). \tag{A18}$$

Again we can exploit the periodicity of the system to reduce the integral to a single unit cell and solve it explicitly. As the final result we get

$$\langle\hat{\sigma}_x\rangle = \frac{\beta^2-1}{\beta^2+1} = -A \tag{A19}$$

### 4. Comparison between stripe and single-minimum phase

A Bose gas with spin-orbit coupling can form the stripe phase, the single-minimum phase, and the polarized phase. We are only able to compare the stripe phase and the single-minimum phase, because we are working with a spin-averaged approach [38] and spin-independent interaction. For a full phase diagram and thus also the transition to the polarized phase as in [20], we would need to employ a spin-sensitive approach [62], which is beyond the scope of this paper and left for future investigation. Whether the stripe phase or the single-minimum phase is energetically lower is determined by comparing HNC-EL/0 energies as a function of $\Omega$ in both phases. The intersection of those two lines gives the value $\Omega_{\rm crit}$. For low $\rho_0$ this intersection becomes very flat as seen in Fig. 5, which makes the determination of the crossing point prone to errors.

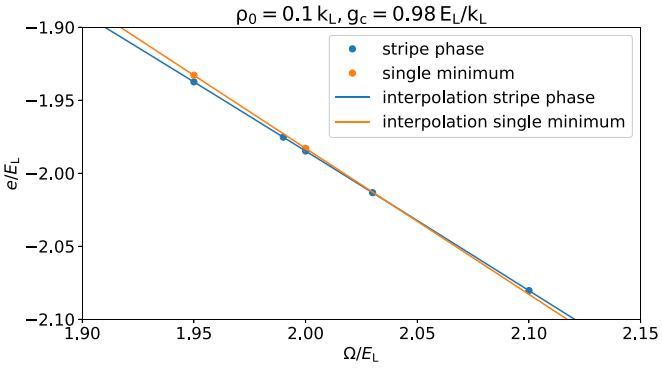


FIG. 5. Energy per particle as a function of $\Omega$. The data for the energy of the single-minimum phase is interpolated linearly and the data for the energy of the stripe phase is interpolated quadratically.

Without interactions the stripe phase is energetically favored over the homogeneous single-minimum phase all the way up to $\Omega = 2E_L$. With the inclusion of interactions, the mean-field approach predicts that this first order phase transition occurs already below $\Omega = 2E_L$ [12]. We check this prediction with HNC-EL/0 and determine the point of the transition by comparing the energy of the stripe phase with the energy of the single-minimum phase phase. Both phases are metastable, i.e., stable against infinitesimal density fluctuations for all $\Omega$, hence we have no problem getting converged HNC-EL/0 results for both phases. With a mean-field approach the transition occurs at

$$\frac{\Omega_{\rm crit}^{\rm MF}}{E_L} = 2\left(1+\frac{g_c\rho_0}{4E_L}\right) - 2\left[\left(1+\frac{g_c\rho_0}{4E_L}\right)\frac{g_c\rho_0}{4E_L}\right]^{1/2}. \tag{A20}$$

Figure 6 shows that $\Omega_{\rm crit}$ for HNC-EL/0 is higher than $\Omega_{\rm crit}^{\rm MF}$ especially in the strongly correlated regime of low density. This reveals a stabilization of the stripe phase due to quantum fluctuations, described by the pair correlations $u(x,x')$ in the

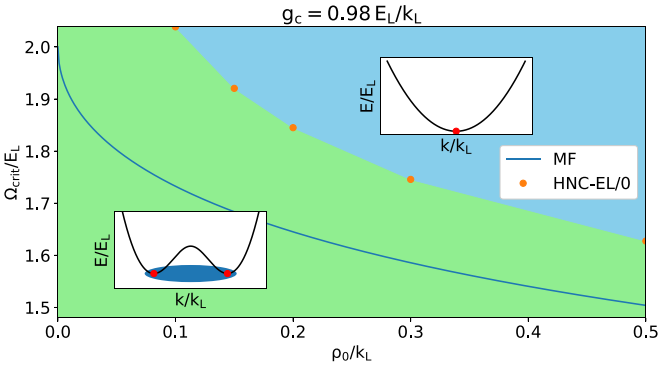


FIG. 6. Energy comparison of unpolarized spin-orbit coupled 1D Bose gas for $g_c = 0.98E_L/k_L$. $\Omega_{\rm crit}$ marks the transition from the stripe phase (green) to the single-minimum phase (blue) as a function of density $\rho_0/k_L$. The blue line is the mean-field result [12]. HNC-EL/0 predicts a stabilization of the stripe phase due to quantum fluctuations beyond the noninteracting limit of $\Omega = 2E_L$.

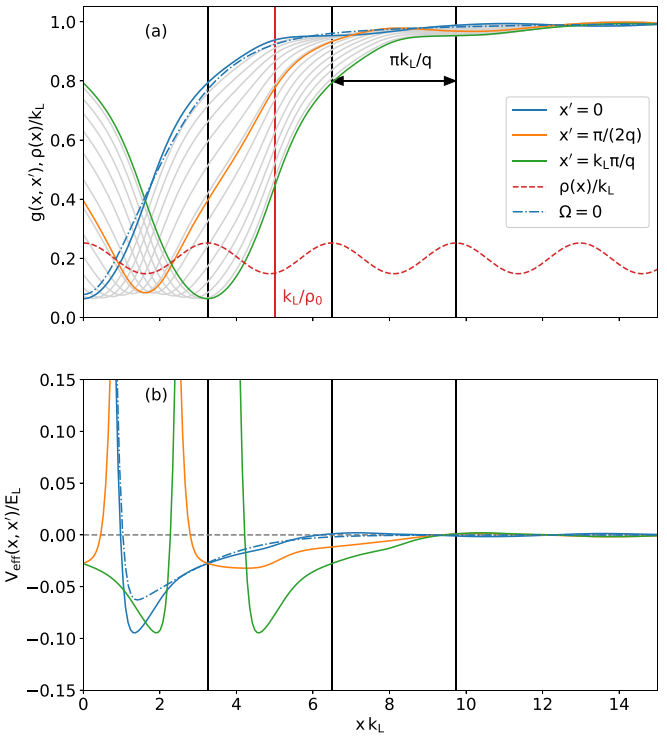


FIG. 7. Pair-distribution function $g(x, x')$ (a) and $V_{\text{eff}}(x, x')$ (b) as a function of $x$ for all $x'$, $\Omega = 0.5E_{\text{L}}$, $\rho_0 = 0.2k_{\text{L}}$, and $g_{\text{c}} = 9.28E_{\text{L}}/k_{\text{L}}$.

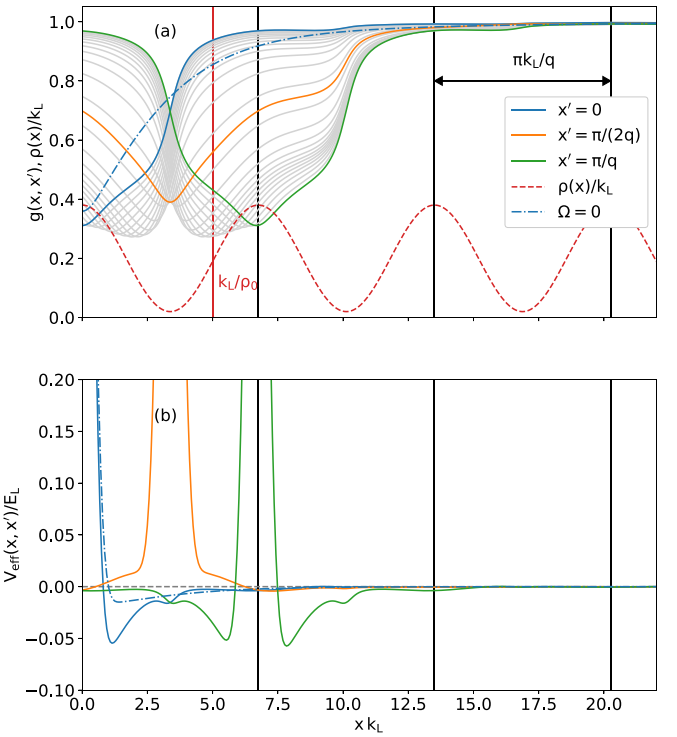


FIG. 9. Pair-distribution function $g(x, x')$ (a) and $V_{\text{eff}}(x, x')$ (b) as a function of $x$ for all $x'$, $\Omega = 1.9E_{\text{L}}$, $\rho_0 = 0.2k_{\text{L}}$, and $g_{\text{c}} = 0.98E_{\text{L}}/k_{\text{L}}$.

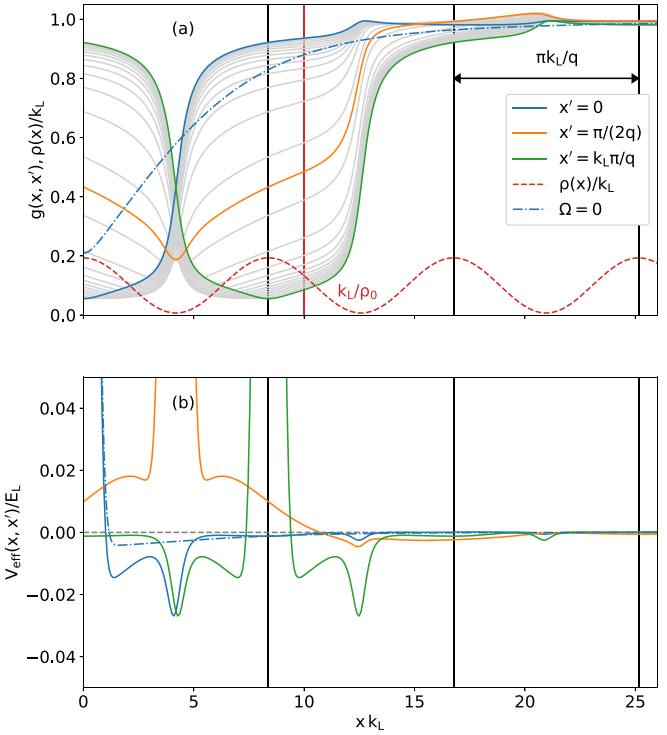


FIG. 8. Pair-distribution function $g(x, x')$ (a) and $V_{\text{eff}}(x, x')$ (b) as a function of $x$ for all $x'$, $\Omega = 1.9E_{\text{L}}$, $\rho_0 = 0.1k_{\text{L}}$, and $g_{\text{c}} = 0.98E_{\text{L}}/k_{\text{L}}$.

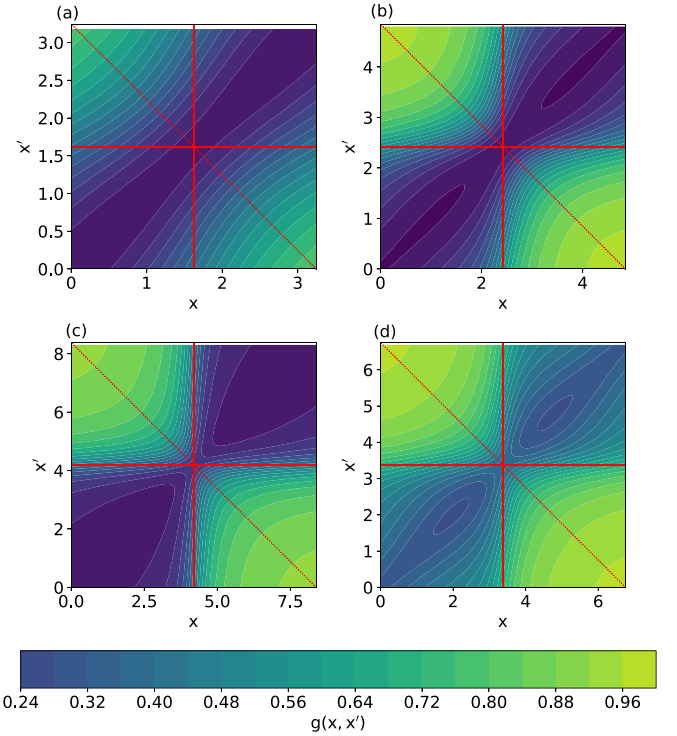


FIG. 10. Pair-distribution function $g(x, x')$ in the first unit cell. All plots are for $\rho_0 = 0.2k_{\text{L}}$ except for panel (c). In the top plots [(a),(b)] $g_{\text{c}} = 9.28E_{\text{L}}/k_{\text{L}}$ and in the bottom plots [(c),(d)] $g_{\text{c}} = 0.98E_{\text{L}}/k_{\text{L}}$.

Jastrow-Feenberg ansatz (3). A similar observation was made with quantum Monte Carlo methods in 3D [20].

### 5. Pair-distribution functions

In Figs. 7, 8, and 9 pair-distribution functions $g(x, x')$ and their effective interactions $V_{\rm eff}(x, x')$ are depicted for different combinations of $\Omega$, $\rho_0$, and $g_c$ [$g(x, x')$ in Figs. 7 and 8 are also shown in panels (a) and (c) of Fig. 3 in the main text, but we show them again here for comparison with $V_{\rm eff}(x, x')$]. In all cases $V_{\rm eff}(x, x')$ has an attractive well for a distance smaller than the period of the density oscillation; as explained in the main text this causes the decrease of this period. Figure 9 shows $g(x, x')$ for an intermediate choice of $\Omega$, $\rho_0$, and $g_c$ that lies between panels (b) and (c) of Fig. 3 in the main text, see corresponding discussion.

Figure 10 shows all pair-distribution functions again as contour plots, which might be a preferable representation for some readers.


[1] Y. A. Bychkov and E. I. Rashba, Oscillatory effects and the magnetic susceptibility of carriers in inversion layers, J. Phys. C **17**, 6039 (1984).

[2] G. Dresselhaus, Spin-orbit coupling effects in zinc blende structures, Phys. Rev. **100**, 580 (1955).

[3] T. D. Stanescu, B. Anderson, and V. Galitski, Spin-orbit coupled Bose-Einstein condensates, Phys. Rev. A **78**, 023616 (2008).

[4] Y.-J. Lin, R. L. Compton, A. R. Perry, W. D. Phillips, J. V. Porto, and I. B. Spielman, Bose-Einstein Condensate in a Uniform Light-Induced Vector Potential, Phys. Rev. Lett. **102**, 130401 (2009).

[5] Y.-J. Lin, K. Jiménez-García, and B. I. Spielman, Spin-orbit-coupled Bose-Einstein condensates. Nature **471**, 83 (2011).

[6] J.-Y. Zhang, S.-C. Ji, Z. Chen, L. Zhang, Z.-D. Du, B. Yan, G.-S. Pan, B. Zhao, Y.-J. Deng, H. Zhai, S. Chen, and J.-W. Pan, Collective Dipole Oscillations of a Spin-Orbit Coupled Bose-Einstein Condensate, Phys. Rev. Lett. **109**, 115301 (2012).

[7] T. A. Sedrakyan, A. Kamenev, and L. I. Glazman, Composite fermion state of spin-orbit-coupled bosons, Phys. Rev. A **86**, 063639 (2012).

[8] D. L. Campbell and I. B. Spielman, Rashba realization: Raman with RF, New J. Phys. **18**, 033035 (2016).

[9] B. M. Anderson, G. Juzeliunas, V. M. Galitski, and I. B. Spielman, Synthetic 3D Spin-Orbit Coupling, Phys. Rev. Lett. **108**, 235301 (2012).

[10] T.-L. Ho and S. Zhang, Bose-Einstein Condensates with Spin-Orbit Interaction, Phys. Rev. Lett. **107**, 150403 (2011).

[11] S.-K. Yip, Bose-Einstein condensation in the presence of artificial spin-orbit interaction, Phys. Rev. A **83**, 043616 (2011).

[12] Y. Li, L. P. Pitaevskii, and S. Stringari, Quantum Tricriticality and Phase Transitions in Spin-Orbit Coupled Bose-Einstein Condensates, Phys. Rev. Lett. **108**, 225301 (2012).

[13] Q.-Q. Lü and D. E. Sheehy, Density profiles and collective modes of a Bose-Einstein condensate with light-induced spin-orbit coupling, Phys. Rev. A **88**, 043645 (2013).

[14] Z.-Q. Yu, Ground-state phase diagram and critical temperature of two-component Bose gases with Rashba spin-orbit coupling, Phys. Rev. A **87**, 051606(R) (2013).

[15] Z.-F. Yu and J.-K. Xue, The phase diagram and stability of trapped *D*-dimensional spin-orbit coupled Bose-Einstein condensate, Sci. Rep. **7**, 15635 (2017).

[16] A. Ambrosetti, F. Pederiva, E. Lipparini, and S. Gandolfi, Quantum Monte Carlo study of the two-dimensional electron gas in presence of Rashba interaction, Phys. Rev. B **80**, 125306 (2009).

[17] A. Ambrosetti, F. Pederiva, and E. Lipparini, Quantum Monte Carlo study of circular quantum dots in presence of Rashba interaction, Phys. Rev. B **83**, 155301 (2011).

[18] A. Ambrosetti, P. L. Silvestrelli, F. Toigo, L. Mitas, and F. Pederiva, Variational Monte Carlo for spin-orbit interacting systems, Phys. Rev. B **85**, 045115 (2012).

[19] J. Sánchez-Baena, J. Boronat, and F. Mazzanti, Diffusion Monte Carlo methods for spin-orbit-coupled ultracold Bose gases, Phys. Rev. A **98**, 053632 (2018).

[20] J. Sánchez-Baena, J. Boronat, and F. Mazzanti, Supersolid stripes enhanced by correlations in a Raman spin-orbit-coupled system, Phys. Rev. A **101**, 043602 (2020).

[21] W. S. Cole, S. Zhang, A. Paramekanti, and N. Trivedi, Bose-Hubbard Models with Synthetic Spin-Orbit Coupling: Mott Insulators, Spin Textures, and Superfluidity, Phys. Rev. Lett. **109**, 085302 (2012).

[22] J. Li, W. Huang, B. Shteynas, S. Burchesky, F. Ç. Top, E. Su, J. Lee, A. O. Jamison, and W. Ketterle, Spin-Orbit Coupling and Spin Textures in Optical Superlattices, Phys. Rev. Lett. **117**, 185301 (2016).

[23] R. Liao, Searching for Supersolidity in Ultracold Atomic Bose Condensates with Rashba Spin-Orbit Coupling, Phys. Rev. Lett. **120**, 140403 (2018).

[24] T. M. Bersano, J. Hou, S. Mossman, V. Gokhroo, X.-W. Luo, K. Sun, C. Zhang, and P. Engels, Experimental realization of a long-lived striped Bose-Einstein condensate induced by momentum-space hopping, Phys. Rev. A **99**, 051602(R) (2019).

[25] X.-W. Luo and C. Zhang, Tunable spin-orbit coupling and magnetic superstripe phase in a Bose-Einstein condensate, Phys. Rev. A **100**, 063606 (2019).

[26] A. Putra, F. Salces-Cárcoba, Y. Yue, S. Sugawa, and I. B. Spielman, Spatial Coherence of Spin-Orbit-Coupled Bose Gases, Phys. Rev. Lett. **124**, 053605 (2020).

[27] J.-R. Li, J. Lee, W. Huang, S. Burchesky, B. Shteynas, Ç. F. Top, O. A. Jamison, and W. Ketterle, A stripe phase with supersolid properties in spin-orbit-coupled Bose-Einstein condensates, Nature **543**, 91 (2017).

[28] C. Hickey and A. Paramekanti, Thermal Phase Transitions of Strongly Correlated Bosons with Spin-Orbit Coupling, Phys. Rev. Lett. **113**, 265302 (2014).

[29] Y. Zhang, L. Mao, and C. Zhang, Mean-Field Dynamics of Spin-Orbit Coupled Bose-Einstein Condensates, Phys. Rev. Lett. **108**, 035302 (2012).

[30] G. I. Martone, Y. Li, and S. Stringari, Approach for making visible and stable stripes in a spin-orbit-coupled Bose-Einstein superfluid, Phys. Rev. A **90**, 041604(R) (2014).

[31] L. P. Pitaevskii and S. Stringari, *Bose-Einstein Condensation*, International Series of Monographs on Physics (Clarendon Press, Oxford, 2003).

[32] E. Krotscheck, Theory of correlated basis functions, in *Introduction to Modern Methods of Quantum Many–Body Theory and*

*their Applications*, Advances in Quantum Many-Body Theory Vol. 7, edited by A. Fabrocini, S. Fantoni, and E. Krotscheck (World Scientific, Singapore, 2002), pp. 267–330.

[33] A. Polls and F. Mazzanti, Microscopic description of quantum liquids, in *Introduction to Modern Methods of Quantum Many-Body Theory and Their Applications*, Series on Advances in Quantum Many Body Theory Vol. 7, edited by A. Fabrocini, S. Fantoni, and E. Krotscheck (World Scientific, Singapore, 2002), p. 49.

[34] E. Krotscheck, M. D. Miller, and J. Wojdylo, Variational approach to the many-boson problem in one dimension, Phys. Rev. B **60**, 13028 (1999).

[35] E. Krotscheck and M. D. Miller, Properties of $^4$He in one dimension, Phys. Rev. B **60**, 13038 (1999).

[36] E. Krotscheck, G. X. Qian, and W. Kohn, Theory of inhomogeneous quantum systems. I. Static properties of Bose fluids, Phys. Rev. B **31**, 4245 (1985).

[37] E. Krotscheck, Inhomogeneous quantum liquids: Statics, dynamics, and thermodynamics, in *Microscopic Quantum Many-Body Theories and Their Applications*, Lecture Notes in Physics Vol. 510, edited by J. Navarro and A. Polls (Springer, Berlin, 1998), pp. 187–250.

[38] M. Panholzer, The hypernetted chain equations for periodic systems. J. Low Temp. Phys. **187**, 639 (2017).

[39] P. Jeszenszki, A. Y. Cherny, and J. Brand, *s*-wave scattering length of a Gaussian potential, Phys. Rev. A **97**, 042708 (2018).

[40] M. Olshanii, Atomic Scattering In The Presence of an External Confinement and a Gas of Impenetrable Bosons, Phys. Rev. Lett. **81**, 938 (1998).

[41] C. E. Campbell, The structure of quantum fluids, in *Progress in Liquid Physics*, edited by C. A. Croxton (John Wiley & Sons, Ltd., New York, 1978), Chap. 6, pp. 213–308.

[42] E. Feenberg, *Theory of Quantum Fluids* (Academic Press, New York, 1969).

[43] C. A. Melton, M. Zhu, S. Guo, A. Ambrosetti, F. Pederiva, and L. Mitas, Spin-orbit interactions in electronic structure quantum Monte Carlo methods, Phys. Rev. A **93**, 042502 (2016).

[44] J. P. Hansen and I. R. McDonald, *Theory of Simple Liquids* (Elsevier Academic Press, New York, 2006).

[45] M. Girardeau, Relationship between systems of impenetrable bosons and fermions in one dimension, J. Math. Phys. **1**, 516 (1960).

[46] C. J. Pethick and H. Smith, *Bose–Einstein Condensation in Dilute Gases*, 2nd ed. (Cambridge University Press, Cambridge, 2008).

[47] The energy obtained by HNC-EL/0 for impenetrable point-like bosons without SOC is about 25% higher than the exact result for $\rho_0 = 0.2k_{\mathrm{L}}$. This can be systematically improved by the inclusion of elementary diagrams.

[48] X. Cui and T.-L. Ho, Spin-orbit-coupled one-dimensional Fermi gases with infinite repulsion, Phys. Rev. A **89**, 013629 (2014).

[49] Q. Guan and D. Blume, Spin structure of harmonically trapped one-dimensional atoms with spin-orbit coupling, Phys. Rev. A **92**, 023641 (2015).

[50] An expression for the induced interaction $w_{\mathrm{I}}(x, x')$ can be found in [38], where $v_{\mathrm{F}}$ is to be set to 0.

[51] L. Salasnich and B. A. Malomed, Localized modes in dense repulsive and attractive Bose-Einstein condensates with spin-orbit and Rabi couplings, Phys. Rev. A **87**, 063625 (2013).

[52] D. A. Zezyulin, R. Driben, V. V. Konotop, and B. A. Malomed, Nonlinear modes in binary bosonic condensates with pseudo–spin-orbital coupling, Phys. Rev. A **88**, 013607 (2013).

[53] E. Chiquillo, Harmonically trapped attractive and repulsive spin-orbit and Rabi coupled Bose-Einstein condensates, J. Phys. A **50**, 105001 (2017).

[54] D. Hufnagl and R. E. Zillich, Stability and excitations of a bilayer of strongly correlated dipolar bosons, Phys. Rev. A **87**, 033624 (2013).

[55] E. Krotscheck, Optimal three-body correlations and elementary diagrams in liquid $^4$He, Phys. Rev. B **33**, 3158 (1986).

[56] Z. Chen and H. Zhai, Collective-mode dynamics in a spin-orbit-coupled Bose-Einstein condensate, Phys. Rev. A **86**, 041604(R) (2012).

[57] P.-S. He, R. Liao, and W.-M. Liu, Feynman relation of Bose-Einstein condensates with spin-orbit coupling, Phys. Rev. A **86**, 043632 (2012).

[58] L. Zhang, J.-Y. Zhang, S.-C. Ji, Z.-D. Du, H. Zhai, Y. Deng, S. Chen, P. Zhang, and J.-W. Pan, Stability of excited dressed states with spin-orbit coupling, Phys. Rev. A **87**, 011601(R) (2013).

[59] M. Saarela, Elementary excitations and dynamic structure of quantum fluids, in *Introduction to Modern Methods of Quantum Many-Body Theory and Their Applications*, Series on Advances in Quantum Many Body Theory Vol. 7, edited by A. Fabrocini, S. Fantoni, and E. Krotscheck (World Scientific, Singapore, 2002), p. 205.

[60] A. Macia, D. Hufnagl, F. Mazzanti, J. Boronat, and R. E. Zillich, Excitations and Stripe Phase Formation in a Two-Dimensional Dipolar Bose Gas with Tilted Polarization, Phys. Rev. Lett. **109**, 235307 (2012).

[61] M. Rader, M. Hebenstreit, and R. E. Zillich, Multicomponent correlated-basis-function method and its application to multilayered dipolar Bose gases, Phys. Rev. A **95**, 033625 (2017).

[62] C. Staudinger, F. Mazzanti, and R. E. Zillich, Self-bound Bose mixtures, Phys. Rev. A **98**, 023633 (2018).